

Numerical modelling of γ -ray emission produced by electrons originating from the magnetospheres of millisecond pulsars in globular clusters

A. Zajczyk^{1,2*}, W. Bednarek³, B. Rudak¹

¹Physics Department, Washington University in St. Louis, 1 Brookings Drive, CB 1105, St. Louis, MO 63130, USA

²Department of Astrophysics, N. Copernicus Astronomical Center, ul. Rzybińska 8, 87-100 Toruń, Poland

³Department of Astrophysics, University of Łódź, ul. Pomorska 149/153, 90-236 Łódź, Poland

Accepted 20... Received 2012

ABSTRACT

Globular clusters are source of γ -ray radiation. At GeV energies, their emission is attributed to magnetospheric activity of millisecond pulsars residing in the clusters. Inverse Compton scattering (ICS) of ambient photon fields on relativistic particles diffusing through cluster environment is thought to be the source of GeV to TeV emission of globular clusters. Using *pair starved polar cap* model γ -ray emission from synthetic millisecond pulsar was modelled. In addition to pulsar emission characteristics, the synthetic pulsar model yielded spectra of electrons escaping pulsar magnetosphere. To simulate γ -ray emission of globular cluster, both products of synthetic millisecond pulsar modelling were used. Gamma-ray spectra of synthetic millisecond pulsars residing in the cluster were summed to produce the magnetospheric component of cluster emission. Electrons ejected by these pulsars were injected into synthetic globular cluster environment. Their diffusion and interaction, both, with cluster magnetic field and ambient photon fields, were performed with Bednarek & Sitarek (2007) model yielding ICS component of cluster emission. The sum of the magnetospheric and ICS components gives the synthetic γ -ray spectrum of globular cluster. The synthetic cluster spectrum stretches from GeV to TeV energies. Detailed modelling was performed for two globular clusters: Terzan 5 and 47 Tucanae. Simulations are able to reproduce (within errors) the shape and the flux level of the GeV part of the spectrum observed for both clusters with the Fermi/LAT instrument. The synthetic flux level obtained in the TeV part of the clusters' spectrum is in agreement with a H.E.S.S. upper limit determined for 47 Tuc, and with emission level recently detected for Ter 5 with H.E.S.S. telescope. The synthetic globular cluster model, however, is not able to reproduce the exact shape of the TeV spectrum observed for Ter 5.

Key words: gamma-rays: theory – globular clusters: individual (Ter 5, 47 Tuc) – pulsars: general – radiation mechanisms: non-thermal

1 INTRODUCTION

Recently, globular clusters (GCs) were established as a source of GeV emission. So far, the LAT instrument onboard the Fermi Space Telescope has detected 15 globular clusters (Abdo et al. 2009a, 2010; Kong et al. 2010; Tam et al. 2011) emitting photons in the energy range from ~ 200 MeV to ~ 50 GeV. All of them are seen as point sources.

For 8 of the γ -ray emitting GCs (Abdo et al. 2010) the placement of the emission is coincident with the position of the clusters. In these cases the observed γ -ray emission

does not vary in time. Moreover, their differential photon spectra can be fitted with a power law with an exponential cut-off. The derived spectral indices are $\Gamma \lesssim 2.0$, and the cut-off energies \mathcal{E}_c fall in the range between 1 GeV and 4.5 GeV. However, for two of these GCs (M62 and NGC 6652) the determined spectral cut-offs are not statistically significant (Abdo et al. 2010). Nonetheless, the observed characteristics of the γ -ray emission of globular clusters resembles that observed for millisecond pulsars (MSPs) detected with the Fermi/LAT instrument at GeV energies (Abdo et al. 2009b). Thus, the population of MSPs residing in the clusters can be responsible for their γ -ray radiation.

* E-mail: azajczyk@physics.wustl.edu

Tam et al. (2011) reported detection of 7 more γ -ray

emitting globular clusters. Interestingly, their γ -ray emission is slightly shifted with respect to the position of the cluster. The extreme case here is NGC 6441 for which the maximum of the GeV emission falls far outside the cluster tidal radius (see fig. 4 of Tam et al. 2011). The γ -ray emission of these 7 GCs does not vary in time. However, in contrast with the clusters detected by Abdo et al. (2010), their observed photon spectra are best fitted by a power law. The exception here is the spectrum of NGC 6441 that is better described by the exponentially cut-off power law (Tam et al. 2011). For two of the clusters (Liller 1 and NGC 6624) the γ -ray spectra extend to energies above 40 GeV. The power-law character of these spectra and their energy extent cannot be solely attributed to the magnetospheric emission of MSPs residing in these clusters. Possibly, the observed emission from these two GCs results from the inverse Compton scattering (ICS) of the ambient photon fields on relativistic electrons injected into globular cluster environment by MSPs.

In addition to the Fermi/LAT detection in the GeV domain, the γ -ray emission at the TeV energies was detected towards Terzan 5 globular cluster (Abramowski et al. 2011). It is slightly extended beyond the GC tidal radius. Moreover, the peak of the emission is significantly shifted with respect to the cluster centre (see fig. 1 of Abramowski et al. 2011). The observed spectrum can be approximated by a power law with a photon spectral index $\Gamma \simeq 2.5$. The ICS photons may substantially contribute to the observed TeV radiation from Terzan 5. However, the ICS origin of TeV emission cannot account for the observed source morphology. Abramowski et al. (2011) give different possible explanations of the TeV radiation detected from the direction of Ter 5. Source coincidence is one of the explored possibilities. In such case the TeV γ -rays could originate from a pulsar wind nebula associated with a radio-quiet pulsar. However, the probability of such scenario is very low. Other possibility is that the TeV emission could have hadronic origin (for details see Abramowski et al. 2011). This scenario could explain the power-law emission spectrum. No TeV emission from the direction of other globular clusters has been detected so far (Anderhub et al. 2009; Aharonian et al. 2009; McCutcheon 2009).

Hui et al. (2011) studied these 15 globular clusters detected in the γ -rays (Abdo et al. 2009a, 2010; Kong et al. 2010; Tam et al. 2011) in search of correlations between the cluster γ -ray luminosity L_γ and various cluster properties. Such correlations could possibly facilitate explanation of the origin of the γ -ray emission of these GCs. Hui et al. (2011) investigated the correlation between L_γ of the GC and two-body encounter rate Γ_c , metallicity $[\text{Fe}/\text{H}]$, absolute visual magnitude, and photon densities of the infrared and the optical Galactic background. The weakest correlation is found between L_γ and the absolute visual magnitude of the cluster. However, strong correlation is found between L_γ and the two-body encounter rate and also the metallicity of the cluster. The reported correlations are consistent with results previously found by Hui et al. (2010) and Abdo et al. (2010). Moreover, they find that the cluster γ -ray luminosity increases with the increase of the density of the background photon fields, both the optical and the infrared ones. The correlation of L_γ and Γ_c suggests that the γ -ray emission of globular clusters is related to the population of objects formed through dynamical interactions in the cluster. This

in turn leads to the conclusion that L_γ depends on the number of MSPs residing in the cluster (Abdo et al. 2010).

Metal-rich globular clusters are more likely to contain bright low-mass X-ray binaries (LMXBs). As proposed by Ivanova (2006), this can be related to the different stellar structure of main sequence donors with masses between $\sim 0.85M_\odot$ and $\sim 1.25M_\odot$. Metal-poor main-sequence stars do not have an outer convective zone, while metal-rich ones do. Absence of the convective zone shuts down magnetic braking, which in turn makes orbital shrinkage in these binaries less efficient. Thus, preventing them from becoming bright X-ray sources, while opposite is the case for binaries with metal-rich main-sequence donors. As low-mass X-ray binaries are thought to be progenitors of MSPs, higher probability of LMXBs formation for metal-rich globular clusters translates into a higher formation rate of MSPs for these clusters. Thus, the observed correlation between L_γ and $[\text{Fe}/\text{H}]$ can link the origin of the γ -ray emission in GCs to the population of MSPs.

The observed correlation between L_γ and the density of the photon fields cannot be accounted for if the γ -ray radiation would originate solely from the magnetospheric activity of MSPs. However, such correlation is expected when the γ -rays are produced via ICS. Then the emitted power in ICS process is directly proportional to the energy density of the ambient photon field. The correlations found by Hui et al. (2011) (and also Hui et al. 2010; Abdo et al. 2010) suggest that the interplay between the number of MSPs and the density of the background photon fields determines the γ -ray luminosity of globular clusters.

2 THEORETICAL APPROACH TO γ -RAY EMISSION OF GLOBULAR CLUSTERS

In the past years, γ -ray emission from globular clusters was modelled assuming it results from either combined magnetospheric radiation of millisecond pulsars residing in a cluster, or from IC scattering of different photon fields on relativistic electrons diffusing through GC interior.

The latter scenario was studied in detail by Bednarek & Sitarek (2007, hereafter BS07). In their model, BS07 assumed that relativistic electrons originate either in magnetospheres of pulsars populating a globular cluster or are accelerated at the shock waves arising from collisions of pulsar winds. In the first case BS07 assumed monoenergetic spectra for the electrons; in the second case they used power-law spectra. In both cases, after being injected into the cluster environment the relativistic electrons diffuse through the cluster interacting with its magnetic field. Moreover, on their way out electrons up-scatter photons arising from stellar population in the cluster and photons of the cosmic microwave background (CMB). The modelling of BS07 predicts γ -ray spectra of GCs spanning from GeV to TeV energies.

Similarly to BS07, Cheng et al. (2010) modelled γ -ray emission from globular clusters as arising from ICS processes taking place in the globular cluster environment. However, it was assumed that the relativistic electrons originate only from magnetospheres of millisecond pulsars residing in the cluster. The injected electron spectra were monoenergetic. The relativistic leptons in the model of Cheng et al. (2010)

up-scatter not only the stellar photons and the CMB, but also soft photons originating in the Galaxy (i.e. infrared background and stellar photons from the galactic disk). The resultant γ -ray emission spans GeV to sub-TeV energies. It is important to point out that the model of Cheng et al. (2010) predicts rather high sub-TeV flux for globular clusters. Moreover, it also predicts that the γ -ray emission should extend beyond the cores of GCs (a radius > 10 pc).

Venter et al. (2009) assumed that both processes, ICS and magnetospheric γ -ray emission of millisecond pulsars, contribute to the overall γ -ray brightness of globular clusters. Under assumption that an accelerating electric field in the magnetospheres of MSPs is unscreened (Muslimov & Tsygan 1992; Harding & Muslimov 1998) due to insufficient pair creation, γ -ray emission from MSPs was simulated. In their work, Venter et al. (2009) used population of cluster MSPs as a sole source of relativistic electrons in the GC environment. The energy spectra of electrons injected into the cluster were computed using the same model of the pulsar magnetosphere as the one used for simulating γ -ray emission of MSPs. Using Monte Carlo method, average cumulative magnetospheric spectrum and cumulative electron injection spectrum originating from 100 MSPs were calculated. This allowed for calculating GeV-to-TeV spectra for globular clusters 47 Tuc and Ter 5. Similarly to BS07, to produce ICS component Venter et al. (2009) up-scattered the stellar photons and the CMB photons.

We note that while modelling of GeV-TeV spectral characteristics of GCs puts constraints on the possible number of MSPs populating the cluster and on the cluster magnetic field (given energy densities of ambient photon fields and diffusion coefficients; e.g. Venter et al. 2009), X-ray energy domain yields additional constraints on physical properties of GC. In particular, Buesching et al. (2012) modelled synchrotron emission maps at radio and X-ray energies for Terzan 5. Comparison of the modelled X-ray emission map with the detected diffuse X-ray emission from Ter 5 (Eger et al. 2010) allowed to put additional constraints on diffusion process of relativistic particles within GC. For more details on the content of GCs, their high energy observations and modelling see recent review by Bednarek (2011).

In this paper we present the results of the numerical modelling of γ -ray radiation from globular clusters. In our study it is assumed (similarly as in Venter et al. (2009)) that the cluster γ -ray emission results from combined magnetospheric activity of millisecond pulsars residing in the cluster, and from ICS scattering of ambient photon fields on relativistic electrons propagating through the cluster. These electrons are injected into the cluster environment by the MSPs. Detailed description of the synthetic millisecond pulsar model used for computing γ -ray spectra of pulsars residing in the cluster and also spectra of electrons ejected from their magnetospheres can be found in Sect. 3. In Sect. 4 details of calculations of synthetic γ -ray spectra of globular clusters are presented. Comparison of the simulations with the existing observational data for selected globular clusters can be found in Sect. 5. Conclusions are given in Sect. 6.

3 NUMERICAL MODEL OF SYNTHETIC MILLISECOND PULSAR

In this section we discuss models of γ -ray production in the open magnetosphere (distances comparable to the light cylinder radius) of pulsars, and motivate why the *pair starved polar cap* model (PSPC; Muslimov & Harding 2004b) is preferred by us for the MSPs residing in globular clusters. We also discuss results of PSPC model that are used to calculate magnetospheric and ICS components to the γ -ray GeV-TeV emission of synthetic globular cluster (Sect. 4).

3.1 Justification for the selected synthetic millisecond pulsar model

In the standard polar cap model approach (see e.g., Harding & Muslimov 1998) the accelerating electric field is being screened out at distances close to the neutron star surface (\sim few stellar radii), which means that the acceleration gap fills only a small fraction of the open magnetosphere. Such description may be applicable to classical pulsars (with ages $\tau_c \lesssim 10^7$ yr) where in their magnetospheres pair production through interaction of curvature and/or inverse Compton scattered photons with the magnetic field is sufficient to completely screen the electric field at low altitudes (see e.g., Muslimov & Harding 2004b). However, the situation is completely different for much older pulsars, including millisecond ones. For these pulsars the primary electrons may keep accelerating and at the same time keep emitting high energy photons up to very high altitudes without significant pair production (see e.g., Muslimov & Harding 2004b; Harding et al. 2005). Harding et al. (2005) show that for millisecond pulsars the primaries can be accelerated up to distances comparable to the light cylinder radius.

The characteristics of some of the γ -ray light curves of the millisecond pulsars and their behaviour with respect to the radio light curves (i.e. misalignment of γ -ray peak and radio peak; Abdo et al. 2009b) seem to favour outer magnetosphere as a region where the γ -rays originate. However, the γ -ray and radio light curve modelling performed by Venter et al. (2009) and Venter et al. (2012) showed that the group of γ -ray bright MSPs is non-uniform in terms of the preferred emission model. Three subclasses can be distinguished - two of the subclasses favour the outer magnetosphere as the place of origin of the γ -ray radiation (either in the framework of the outer gap or the slot gap model). However, there are MSPs whose γ -ray emission can only be explained invoking the extended polar cap model, i.e. the *pair starved polar cap* model (Muslimov & Harding 2004b) where the γ -ray emission is produced in the whole volume of the pulsar open magnetosphere.

In the slot gap model (Muslimov & Harding 2004a) the approximate solution to the accelerating electric field E_{\parallel} suffers from a sign reversal. In the outer gap model non-dipolar magnetic field (Cheng et al. 2000) needs to be invoked in order to obtain copious electron-positron pair creation. In turn, the created pairs are needed to control the gap dimensions. The pair starved polar cap model, similarly to the slot gap model, suffers from the sign reversal in the solution for the unscreened accelerating electric field E_{\parallel} (see Sect. 3.3). Nonetheless in the past years it was widely studied (see e.g.,

Venter et al. 2009, and references therein) in the context of γ -ray emission of millisecond pulsars.

Because properties of MSPs in globular clusters are different from the ones of the field population (Camilo & Rasio 2005) it is justified to suspect that the γ -ray emission mechanism operating in the magnetospheres of these globular cluster MSPs may be different from the one operating in the classical pulsars and/or in the field millisecond pulsars. Thus, in the presented study the *pair starved polar cap* (PSPC) model is chosen to simulate the γ -ray emission of millisecond pulsars.

3.2 Basic assumptions of the synthetic millisecond pulsar model

To simulate the γ -ray emission of millisecond pulsars a 3 dimensional (3D) numerical model of pulsar magnetosphere was used (Dyks 2002). The model operates within a *space charge limited flow* framework. The magnetic field of a pulsar is in the form of a retarded vacuum dipole (Dyks et al. 2004) for which the curvature radii of magnetic field lines are determined in the inertial frame of reference. Moreover, following Dyks & Rudak (2002) the special relativity effects like aberration and time-of-flight delays are treated accordingly throughout the calculations.

Important change introduced into the numerical code was an inclusion of a more realistic description of the electric field $E_{||}$ (for details see Sect. 3.3). It is assumed that acceleration of particles takes place in the whole volume determined by the last open magnetic field lines. The electrons are injected at the polar cap surface at the Goldreich-Julian rate, and they have low initial energy. As there is no screening of the electric field, like in the standard polar cap model (see e.g., Harding & Muslimov 1998), acceleration of the particles takes place even at distances comparable to the light cylinder radius. Such model is called a *pair starved polar cap* model (Muslimov & Harding 2004b). The implemented electric field takes into account the general relativistic effect of dragging of inertial frames (Muslimov & Tsygan 1992; Muslimov & Harding 2004b).

3.3 Structure of the accelerating electric field

In the 3D numerical model of the millisecond pulsar magnetosphere the accelerating electric field $E_{||}$ in the form proposed by Muslimov & Harding (2004b) was implemented. The field itself extends up to the light cylinder and consists of three different prescriptions (E_1 , E_2 and E_3) determining $E_{||}$ at different heights above the pulsar surface.

In the region close to the neutron star surface (further referred to as the *near* regime) the accelerating electric field is described by the formula derived by Muslimov & Tsygan (1992) under assumption that the electric field must disappear at the stellar surface ($E_{||} = 0$):

$$E_1 = -3E_0\theta_0^2 \left\{ \kappa \cos \alpha \sum_{i=1}^{\infty} \frac{4J_0(k_i\xi)}{k_i^3 J_1(k_i)} [1 - e^{-\gamma_i z}] \right. \\ \left. + \theta_0 H(1)\delta(1) \sin \alpha \cos \phi \sum_{i=1}^{\infty} \frac{2J_1(\tilde{k}_i\xi)}{\tilde{k}_i^3 J_2(\tilde{k}_i)} [1 - e^{-\tilde{\gamma}_i z}] \right\}. \quad (1)$$

The above equation is expressed in the *magnetic* coordinate

system (r, θ, ϕ) , where r is the radial distance from the neutron star centre, θ is the magnetic colatitude, and ϕ is the magnetic azimuthal coordinate. This is also the case for all the $E_{||}$ formulae presented in this Section. The angle α in Eq. 1 is the angle between the rotation and the magnetic axis, $\xi \equiv \theta/\theta(\eta)$ is the magnetic colatitude scaled with the polar angle of the last open magnetic field line, $\eta = r/R_{\text{NS}}$ is the radial distance scaled with the star radius, and $z \equiv \eta - 1$ is the altitude above the neutron star surface scaled with the star radius. The electric field is derived using a small-angle approximation, in which the polar angle of the last open magnetic field line $\theta(\eta) \ll 1$. This results in:

$$\theta(\eta) \simeq \theta_0 \sqrt{\eta \frac{f(1)}{f(\eta)}}, \quad \text{where} \quad \theta_0 = \sqrt{\frac{\Omega R_{\text{NS}}}{c f(1)}}. \quad (2)$$

Here θ_0 is the magnetic colatitude (polar angle) of the base of the line at the stellar surface. Other quantities used in Eq. 1 are:

$$E_0 \equiv B_s \frac{\Omega R_{\text{NS}}}{c}, \quad \kappa \equiv \frac{\epsilon I}{M_{\text{NS}} R_{\text{NS}}^2}, \quad \epsilon \equiv \frac{2GM_{\text{NS}}}{c^2 R_{\text{NS}}}, \quad (3)$$

where M_{NS} is the mass of a neutron star, $\epsilon = r_g/R_{\text{NS}}$ is the compactness parameter ($r_g = 2GM_{\text{NS}}/c^2$ is the gravitational radius of a neutron star), and κ is the magnitude of the general relativistic effect of the frame dragging at the stellar surface measured in the stellar angular velocity Ω . The function J_m is a Bessel function of order m . The k_i and \tilde{k}_i are the positive roots of the Bessel functions J_0 and J_1 . Functions γ_i and $\tilde{\gamma}_i$ are defined as:

$$\gamma_i \approx \frac{k_i}{\theta_0(1-\epsilon)^{1/2}}, \quad \text{and} \quad \tilde{\gamma}_i \approx \frac{\tilde{k}_i}{\theta_0(1-\epsilon)^{1/2}}. \quad (4)$$

Formulae for $f(\eta)$, $H(\eta)$ and $\delta(\eta)$ were first defined in Muslimov & Tsygan (1992) and can be found therein. The *near* regime solution E_1 is applicable for altitudes $\eta - 1 \ll 1$.

At moderate heights ($\theta_0 \ll \eta - 1 \ll \frac{c}{\Omega R_{\text{NS}}}$; further referred to as the *moderate* regime) the electric field is given by eq. 14 of Harding & Muslimov (1998):

$$E_2 = -\frac{3}{2}E_0\theta_0^2 \left[\frac{\kappa}{\eta^4} \cos \alpha \right. \\ \left. + \frac{1}{4}\theta(\eta)H(\eta)\delta(\eta)\xi \sin \alpha \cos \phi (1 - \xi^2) \right]. \quad (5)$$

Close to the light cylinder (further referred to as the *far* regime) the electric field is described by eq. 35 of Muslimov & Harding (2004b):

$$E_3 \approx -\frac{3}{16} \left(\frac{\Omega R_{\text{NS}}}{c} \right)^3 \frac{B_s}{f(1)} \left[\kappa \left(1 - \frac{1}{\eta_c^3} \right) (1 + \xi^2) \cos \alpha \right. \\ \left. + \frac{1}{2}(\sqrt{\eta_c} - 1) \left(\frac{\Omega R_{\text{NS}}}{c} \right)^{1/2} \lambda (1 + 2\xi^2) \xi \sin \alpha \cos \phi \right] \\ \times (1 - \xi^2), \quad (6)$$

where $\lambda = H(1)/\sqrt{f(1)}$, and η_c is a radial parameter at which the electric field saturates (Muslimov & Harding 2004a).

In order to obtain a smooth transition between the electric field working in the *moderate* regime (Eq. 5) and the one working in the *far* regime (Eq. 6) the formula proposed by Muslimov & Harding (2004b) is used:

$$E_{||} \simeq E_2 \exp \left[-\frac{\eta - 1}{\eta_c - 1} \right] + E_3. \quad (7)$$

The value of η_c parameter is determined for each magnetic field line separately. Muslimov & Harding (2004b) showed that for millisecond pulsars the best-fit value of η_c falls in the range $\sim 3 - 4$. Moreover, they point out that for a given pulsar spin period the parameter η_c is a function of an inclination α and an azimuthal coordinate ϕ at the polar cap.

In the numerical code before electrons are injected into the pulsar magnetosphere, we find the accelerating electric field solution in the whole volume of the open magnetosphere up to the light cylinder distances. When finding the full $E_{||}$ solution that could accelerate particles also in the distant parts of the magnetosphere (so a combination of Equations 1, 5 and 6 with the use of Eq. 7), following Venter et al. (2009), we require that the resultant electric field:

- should be negative for all η in the range between 1 and η_{LC} , where $\eta_{LC} = r/R_{LC}$;
- should transit from the *near* to the *moderate* $E_{||}$ regime (matching E_1 with E_2) when $E_1 \simeq E_2$;
- should transit from the *moderate* to the *far* $E_{||}$ regime (matching E_2 with E_3) smoothly, which is achieved by applying Eq. 7 and appropriate matching of η_c ;
- should converge to E_3 for the distances close to the light cylinder.

For the implemented electric field (Eq. 1, 5 and 6) a sign reversal of the electric field occurs at some altitude. This happens especially for those magnetic field lines that cross the null-charge surface¹ within the volume of the open magnetosphere limited by the light cylinder radius. When $E_{||}$ changes sign, the particle oscillations occur. In order to alleviate this somewhat problematic situation it is required that $E_{||}$ field is negative for all η . If this condition is not fulfilled for a certain magnetic field line, the line is left out from the calculations so no acceleration of particles takes place along this line. To obtain smooth transition from E_2 to E_3 we take a broader range of possible values of η_c than the one found by Muslimov & Harding (2004b) for millisecond pulsars. The values of η_c are chosen from the range between 1 and 6. In the matching procedure the largest possible value of η_c that ensures the smooth transition between the electric field solutions given by Eqs. 5 and 6 is chosen.

The distribution of the η_c parameter across the polar cap for the case of $B_s = 10^8$ and different values of P and α is presented in Fig. 1. When the inclination increases a region with progressively smaller values of η_c increases at the polar cap side facing away from the rotation axis ($\phi = 180^\circ$). This is true for all presented spin periods. For $\alpha = 80^\circ$ large part of the magnetosphere is excluded from the calculations (no solution of $E_{||}$ is found). Such behaviour results from the fact that when we increase pulsar inclination the magnetic field lines situated in the part of the magnetosphere at large distances from the rotation axis start crossing the null-charge surface. Thus, in order to mitigate the problem of particle oscillations the open magnetic field lines crossing the null-charge surface are excluded from the calculations.

Previously, the γ -ray emission of millisecond pulsars was modelled by e.g. Venter & De Jager (2005) and Zajczyk (2008). Their calculations were carried out in the framework

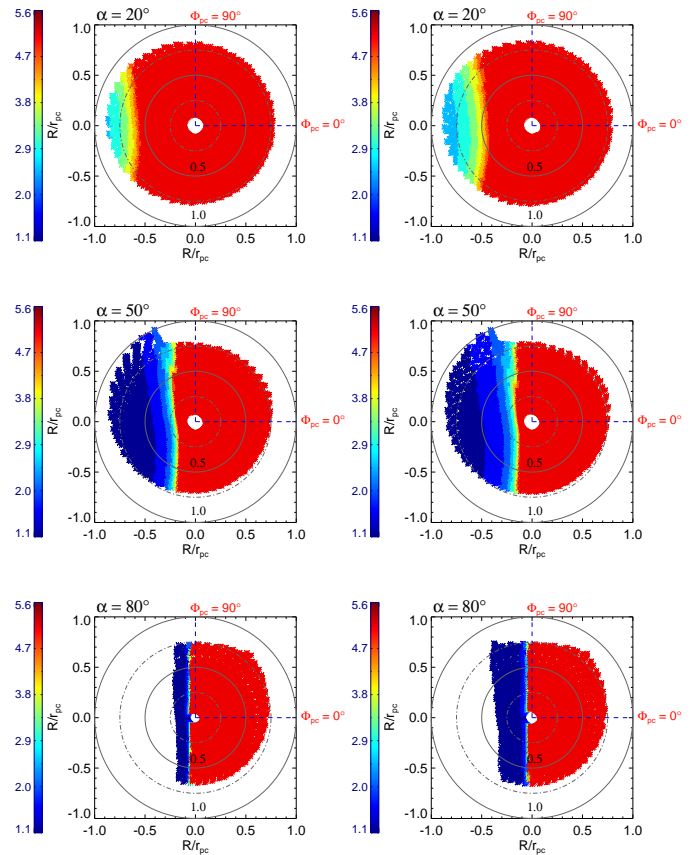


Figure 1. The distribution of η_c parameter across the pulsar polar cap. The images show results for synthetic MSP with $B_s = 10^8$ G. The *left* column shows the case with $P = 1.5$ ms, while the *right* column shows the case with $P = 9.5$ ms. The inclination changes along columns: *top* row $\alpha = 20^\circ$, *middle* row $\alpha = 50^\circ$, and *bottom* row $\alpha = 80^\circ$. Different values of the parameter η_c are colour-coded (see colorbars for the exact values). White regions are those for which no $E_{||}$ solution is found. Small and big solid circle mark the distance across the polar cap equal to $0.5r_{pc}$ and $1.0r_{pc}$, respectively. Here r_{pc} is the polar cap radius. Horizontal red dashed line shows $\phi = 0^\circ$ while vertical one points to $\phi = 90^\circ$ (ϕ is the magnetic azimuth angle).

of the extended polar cap model. However, they considered accelerating electric field $E_{||}$ of the form given by Eqs. 1 and 5. Thus, electrons were accelerated only up to the distances $\ll \eta_{LC}$. Venter et al. (2009) performed the calculations of the γ -ray characteristics of the millisecond pulsars using the pair starved polar cap model, thus including also Eq. 6 in the description of the accelerating electric field. The conditions that need to be met when finding the solution of $E_{||}$ along the magnetic field lines are similar for Venter et al. (2009) and the implementation of the PSPC model presented in this work. However, one difference can be found. In order to match the electric field solutions in the *near - moderate* distance regime Venter et al. (2009) used the approximate formula $\eta_b \approx 1 + 0.0123P^{-0.333}$, where η_b is the distance at which the transition between E_1 and E_2 takes place. In this case, the distance η_b is independent of the position at the polar cap, so the change from E_1 to E_2 for all open magnetic field lines takes place at the same distance from the neutron

¹ *null-charge surface* is the surface in the pulsar magnetosphere separating volumes filled with the particles of opposite charge.

star surface. In the presented study, however, the distance of transition between E_1 and E_2 is determined for each of the magnetic field lines independently. The transition takes place at the distance where the condition of $E_1 \simeq E_2$ is fulfilled. Thus, the transition height from the *near* to *moderate* regime varies across the polar cap. This in turn results in different transition heights from the *moderate* to *far* regime, so the slightly different η_c values, with respect to the ones found by Venter et al. (2009). The general behaviour of the η_c parameter with the increasing inclination is similar in both cases. Additionally, the step in the numerical grid of the η_c values used in the $E_{||}$ calculations has direct impact on the exact distribution of η_c across the polar cap. Thus, the final result is the outcome of the two effects. The observed differences between Venter et al. (2009) and the presented implementation of the PSPC model, though observed, have minor effect on the calculated γ -ray emission characteristic of the synthetic millisecond pulsars.

Having found the accelerating electric field structure across the pulsar magnetosphere, electrons are injected at the polar cap with low initial energy ($\gamma_0 = 10$). The particles are distributed across the polar cap ($\eta = 1$) with the Goldreich-Julian charge density that includes general relativistic corrections (see e.g., Muslimov & Harding 1997; Harding & Muslimov 1998):

$$\begin{aligned} \rho_{\text{GJ}} &= -\frac{\Omega B_s}{2\pi c \tilde{\alpha} \eta^3} \frac{f(\eta)}{f(1)} \left(1 - \frac{\kappa}{\eta^3}\right) \cos \alpha \\ &+ \frac{3}{2} \theta(\eta) H(\eta) \xi \sin \alpha \cos \phi, \end{aligned} \quad (8)$$

where $\tilde{\alpha} \equiv \sqrt{1 - \epsilon/\eta}$ is the red-shift function. Their starting positions coincide with the foot-points of the magnetic field lines. Then the primary particles are being followed in their motion along the magnetic field lines. Moving through the pulsar magnetosphere the particles lose their energy through curvature radiation being at the same time accelerated by the electric field.

The emitted curvature photons interact with magnetic field. However, secondary pairs (electrons and positrons) are produced in insufficient numbers to screen out the electric field. The majority of curvature photons escape pulsar magnetosphere without being absorbed. At the same time, information on their energy and direction of motion is collected to produce photon maps (Dyks 2002), which give information on pulsar emission characteristics (the number of photons $d\dot{N}_\gamma$ radiated per unit time, per unit energy $d\mathcal{E}$, into unit solid angle $d\Omega$). The photon maps are used to obtain pulsar spectra and light curves for different observing angles ζ .

Numerical calculations were performed for discrete distribution of pulsar parameters (P , B_s , α). Pulsar spin period was selected from the set of $P = (1.5, 2.0, 3.5, 5.0, 6.5, 8.0, 9.5)$ ms. Magnetic field values were chosen from the set of $B_s = (1.0, 3.5, 4.5, 5.5, 7.5, 9.0) \times 10^8$ G. Pulsar inclination angle was chosen from a range between 10° and 80° with a step of 10° . Such parameter selection allowed for obtaining 336 different synthetic millisecond pulsar cases. For each modelled case a γ -ray photon map² and

spectrum of electrons ejected from pulsar magnetosphere (Sect. 3.4) were obtained.

3.4 Spectra of electrons ejected from millisecond pulsar magnetosphere

In the calculations we also collect information on the Lorentz factors γ_{el} of the electrons escaping the millisecond pulsar magnetosphere. Examples of the electron ejection spectra in the form $\log_{10}(d\dot{N}_{\text{el}}/dE_{\text{el}})$ versus $\log_{10} \gamma_{\text{el}}$ are presented in Figure 2. The $d\dot{N}_{\text{el}}$ is the number of primary electrons of given energy $E_{\text{el}} = \gamma_{\text{el}} m_{\text{el}} c^2$ (m_{el} is the mass of the electron) escaping pulsar magnetosphere per unit time. For the case of $B_s = 10^8$ G and $\alpha = 20^\circ$ the electron ejection spectra are single-peaked (the *left* column of Fig. 2). The Lorentz factors of the particles contributing to the peak are in the range $\sim 10^{5.5} - 10^7$. For these cases, with the increase of the spin period from 1.5 ms to 9.5 ms the spectral peak becomes flatter and shifts towards the lower values of γ_{el} . For $P = 1.5$ ms the peak centre is at $\gamma_{\text{el}} \sim 10^{6.6}$, while for the case of $P = 9.5$ ms it is at $\gamma_{\text{el}} \sim 10^{6.0}$. With the increase of the inclination a pronounced low energy tail starts to develop, which eventually for slowly rotating synthetic millisecond pulsars (e.g. $P = 5$ ms and 9.5 ms) evolves to form a separate low energy peak. Such double-peaked electron ejection spectrum can be seen for the case of $P = 9.5$ ms and $\alpha = 50^\circ$ (the *middle* plot in the *bottom* row of Fig. 2). Similarly as for the cases with $\alpha = 20^\circ$, with the increasing P the shift of the whole spectrum towards the lower energies is observed for the cases with $\alpha = 50^\circ$ and 80° . For the model with $P = 9.5$ ms and $\alpha = 80^\circ$ this results in the fact that the spectrum spans the range of γ_{el} between $\sim 10^4$ and $\sim 10^6$. The similar behaviour in the electron spectra is also observed for the models with larger values of the magnetic field (Zajczyk 2012). However, the development of the low energy tail followed by the emergence of the low energy peak takes place much later in terms of the pulsar inclination (higher α) and spin period (larger P) than for the low B_s pulsars.

The overall behaviour of the electron ejection spectra is linked to the electric field structure $E_{||}$ in the pulsar magnetosphere (see Sect. 3.3). For a given case with P and B_s the development of the low energy peak in the electron spectrum starts when more $E_{||}$ solutions characterised by the low values of the η_c parameter are found across the magnetosphere. This in turn results in the fact that primary electrons accelerated in different parts of the pulsar magnetosphere reach progressively lower energies at the light cylinder. When the electric field structure (determined by the value of η_c) evolves into the state when within approximately half of the magnetosphere high η_c electric field solutions are found, and the other half is characterised by the very low values of η_c or no solutions at all, then the double-peaked characteristics of the electron ejection spectrum sets in. Such situation happens exactly when the inclination becomes $> 40^\circ$ (Fig. 1). For a given case with B_s and α as the pulsar period increases the magnitude of the electric

² *photon map* yields information on pulsar emission characteristics (the number of photons radiated per unit time, per unit energy, into unit solid angle) as a function of pulsar rotation phase

and viewing angle ζ (Dyks 2002). Pulsar emission spectrum for selected ζ is obtained through integrating strip of the photon map $\Delta\zeta$ wide over the pulsar rotation phase.

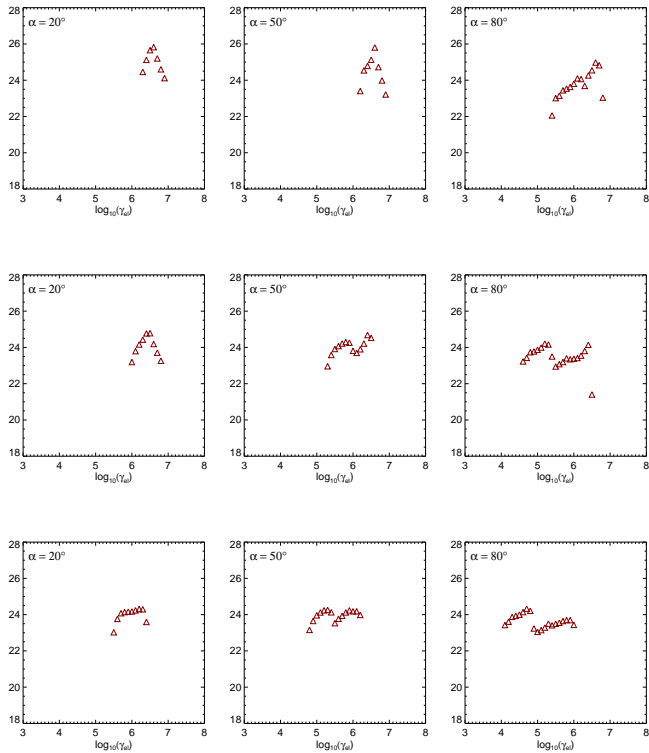


Figure 2. Spectra of electrons escaping through light cylinder for the model with $B_s = 10^8$ G. The Y-axis in each of the subfigures shows $\log_{10}(d\dot{N}_{el}/dE_{el})$ [$s^{-1}MeV^{-1}$]. Spin period P of 1.5, 5.0 and 9.5 ms is presented in the *top*, *middle* and *bottom* row, respectively. Inclination of the pulsar α changes from 20° , 50° to 80° from the *left* column to the *right* one.

field decreases. Thus, on average the primary electrons reach smaller energies at the light cylinder and the whole ejection spectrum moves towards lower values of γ_{el} . Finally, when the pulsar magnetic field strength is increased, the average magnitude of the electric field in the pulsar magnetosphere is increased. The previously described double-peaked spectral behaviour is also present for high B_s cases. However, it becomes pronounced only for slowly rotating ($P > 5$ ms) and highly inclined ($\alpha > 50^\circ$) synthetic pulsars because of the much larger average magnitude of the electric field. For the same reason, the spectrum shift towards lower electron energies is far less severe for the high magnetic field cases ($B_s = 9 \times 10^8$ G), where the low energy end of the spectrum shifts only to $\gamma_{el} \sim 10^5$. For the low magnetic field cases ($B_s = 10^8$ G) the low energy end of the ejection spectrum can shift even to $\gamma_{el} \sim 10^4$.

4 GAMMA-RAY EMISSION OF SYNTHETIC GLOBULAR CLUSTER

Globular clusters have recently been established as a source of the γ -ray radiation (see Sect. 1). Their high energy emission is attributed to the ensemble of millisecond pulsars residing in their cores. Combined magnetospheric activity of the millisecond pulsar population is thought to be the source of the cluster emission above 100 MeV. The spectral shapes

of the radiation observed for GCs (Abdo et al. 2009a, 2010; Kong et al. 2010; Tam et al. 2011) seem to confirm this scenario. The relativistic electrons injected into the cluster environment by the MSPs can up scatter the ambient photon fields (cosmic microwave background, infrared background, and starlight either originating from stellar population in the globular cluster or from stars in the Galaxy). This inverse Compton scattering scenario has been proposed to explain the GCs γ -ray emission in the GeV and TeV energy range (Bednarek & Sitarek 2007; Cheng et al. 2010; Venter et al. 2009). The observational properties of the γ -ray emission of GCs cannot be explained solely with the magnetospheric activity scenario or the ICS scenario. Thus, most probably the interplay between the two models gives rise to the overall GeV and TeV emission of the globular clusters (see Sect. 1 for more details).

4.1 Numerical scheme of the synthetic globular cluster

In order to simulate the γ -ray emission of a synthetic globular cluster both the magnetospheric activity of the population of millisecond pulsars residing in the cluster, and also the ICS scenario is taken into account. The magnetospheric component (Sect. 4.2) is constructed using the results of the *pair starved polar cap* model calculations for different cases of millisecond pulsars (Sect. 3.3). The ICS component is calculated in two steps, first a cumulative spectrum of electrons injected by ensemble of synthetic millisecond pulsars into the cluster environment is computed. The cumulative electron spectrum is constructed using the electron ejection spectra calculated with the *pair starved polar cap model* (see Sects. 3.4). Later, the cumulative spectrum is fed into the numerical model of the cluster (BS07) to produce the ICS radiation (Sect. 4.3).

The numerical procedure that calculates the γ -ray spectrum originating from the ensemble of millisecond pulsars residing in the core of the synthetic cluster, and also the cumulative spectrum of electrons ejected from the magnetospheres of those synthetic MSPs is written in the IDL language.

It is assumed that the number of millisecond pulsars residing in the synthetic cluster is N_{PSR} . These pulsars reside in the cluster core, which in the numerical calculations is resolved assuming that these pulsars are concentrated in one point placed in the cluster centre. In the first step, the basic parameters (a spin period P , a magnetic field strength B_s and an inclination angle α) are selected for each of the millisecond pulsars residing in the modelled cluster. The values of these parameters are randomly selected from the discrete distribution determined by the synthetic MSP population in the database (Sect. 3.3). The random selection is performed with the IDL function `randomu` (Park & Miller 1988).

4.2 Magnetospheric emission of the population of millisecond pulsars in the cluster

Having selected basic parameters (P , B_s , α) that characterise each of N_{PSR} millisecond pulsars populating our synthetic globular cluster, we are ready to compute the magnetospheric contribution of the ensemble of MSPs to the high

energy emission of the synthetic cluster. Each of the selected MSPs emits high energy photons originating in the radiation processes that take place in the pulsar magnetospheres. As already discussed in Sect. 3, in the PSPC model only curvature photons are emitted. **Within the framework of the studied model and the selected range of pulsar parameters (P , B_s , α) there is no additional contribution (with respect to the curvature radiation) at the GeV energy range from synchrotron radiation due to secondary pairs (see e.g., Rudak & Dyks 1999). Moreover, any synchrotron radiation due to cyclotron resonant absorption of radio waves is beyond the scope of the studied model.**

To create the cumulative magnetospheric contribution from the millisecond pulsars, first a viewing angle ζ had to be selected for each pulsar. Its value is randomly selected from the $\sin \zeta$ distribution. Having selected the viewing angle, the observed γ -ray spectrum is constructed for each millisecond pulsar populating the modelled cluster:

$$F_{\text{obs}}(\zeta; \mathcal{E}) = \frac{1}{2\pi D^2} \int_0^{2\pi} \mathcal{E} \frac{d\dot{N}_\gamma}{d\mathcal{E}d\Omega} d\varphi, \quad (9)$$

where ζ is the randomly selected viewing angle, φ is the pulsar rotation phase and D is a distance to the simulated cluster. This in turn allows for computing the overall millisecond pulsar magnetospheric contribution to the observed γ -ray emission of the synthetic cluster:

$$F_{N_{\text{PSR}}}(\mathcal{E}) = \sum_{k=1}^{N_{\text{PSR}}} F_{\text{obs},k}(\zeta; \mathcal{E}). \quad (10)$$

In the *left* column of Fig. 3 examples of the cluster γ -ray spectra resulting *only* from the magnetospheric emission of population of millisecond pulsars are presented. In the *top left* panel of Fig. 3 one thousand cluster γ -ray spectra in the form of $\mathcal{E}F_{N_{\text{PSR}}}(\mathcal{E})$ are shown. It is assumed that 20 millisecond pulsars reside in the modelled cluster. The distance to the cluster is 9.6 kpc. The obtained spectral characteristics of the synthetic cluster is diverse both in terms of the photon cut-off energy and the maximum flux density level. The energy of the cut-off \mathcal{E}_{cut} falls in the range between 10^3 MeV and $\sim 5 \times 10^4$ MeV. The cluster spectra characterised by the lowest value of \mathcal{E}_{cut} are also the spectra with the lowest maximum flux density level $\sim 10^{-12} \text{ erg}^{-1} \text{ s}^{-1} \text{ cm}^{-2}$. The highest generated maximum flux density level is $\sim 10^{-10} \text{ erg}^{-1} \text{ s}^{-1} \text{ cm}^{-2}$. Assuming that there are only 20 pulsars in the cluster we are able to generate the magnetospheric γ -ray spectra of the globular cluster that differ by two orders of magnitude in terms of the flux density level. In the *bottom left* panel of Fig. 3 three hundred cluster γ -ray spectra are displayed. The simulated globular cluster harbours $N_{\text{PSR}} = 100$ millisecond pulsars, and is at the distance of 9.6 kpc. The cut-off energies of the simulated magnetospheric cluster spectra span the energy range between $\sim 2 \times 10^3$ MeV and $\sim 2 \times 10^4$ MeV. The maximum level of the flux density varies between $\sim 3 \times 10^{-11} \text{ erg}^{-1} \text{ s}^{-1} \text{ cm}^{-2}$ and $\sim 3 \times 10^{-10} \text{ erg}^{-1} \text{ s}^{-1} \text{ cm}^{-2}$. The comparison of the models presented in the *top left* ($N_{\text{PSR}} = 20$) and in the *bottom left* ($N_{\text{PSR}} = 100$) panel of Fig. 3 shows that the synthetic globular clusters harbouring smaller number of millisecond pulsars can produce similar magnetospheric γ -ray spectra (in terms of the cut-off energy and the flux density level) as

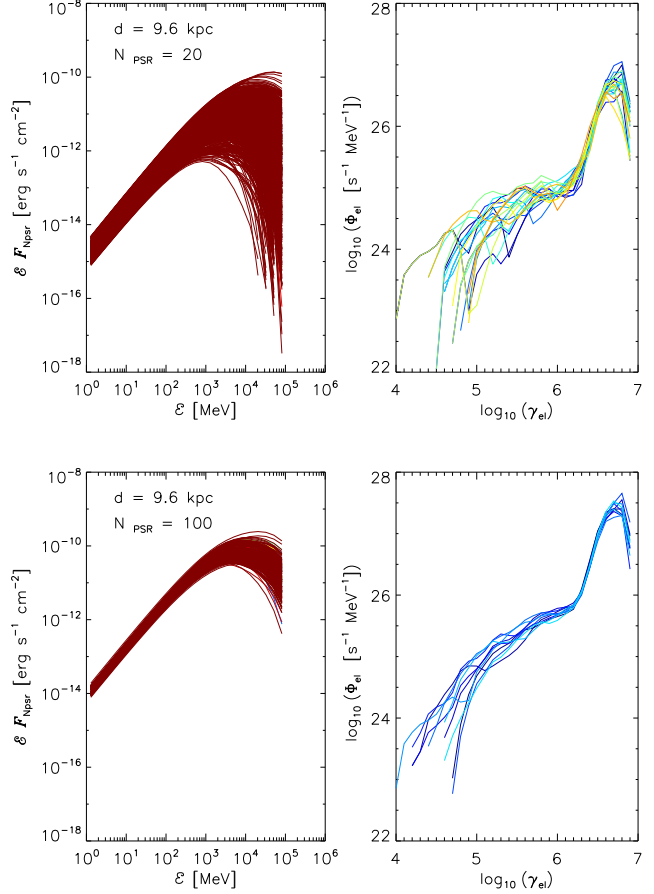


Figure 3. The magnetospheric γ -ray spectra (*left* column) and the cumulative electron spectra (*right* column) computed for different realisations of synthetic globular cluster. The magnetospheric γ -ray spectra are presented in $\mathcal{E}F_{N_{\text{PSR}}}(\mathcal{E})$ form (i.e. a γ -ray flux described by Eq. 10 multiplied by the photon energy \mathcal{E}). The cumulative electron spectra are given by Eq. 12. In the *top* row a modelled GC harbouring 20 millisecond pulsars (N_{PSR}) is presented, while in the *bottom* row a model with $N_{\text{PSR}} = 100$ is shown. In both cases, the distance to the cluster is taken to be $d = 9.6$ kpc.

the ones produce by the clusters with larger pulsar population.

4.3 ICS component to the γ -ray emission of the synthetic globular cluster

The first step in obtaining an ICS emission component to the γ -ray radiation from globular clusters is creation of a cumulative spectrum of electrons injected by the population of synthetic MSPs into the GC environment. The electron ejection spectrum (see Sect. 3.4) for a given pulsar (P , B_s , α) is independent of a viewing angle, so once we have selected these basic pulsar parameters for all N_{PSR} pulsars in the synthetic globular cluster, we construct the electron ejection spectrum for each synthetic pulsar:

$$\Phi_{\text{el},k}(\gamma_{\text{el}}) = \frac{d\dot{N}_{\text{el}}(k)}{dE_{\text{el}}}, \quad (11)$$

where \dot{N}_{el} is the number of electrons with the energy $E_{\text{el}} = \gamma_{\text{el}} m_{\text{el}} c^2$ ejected from pulsar magnetosphere per unit time. Then to obtain the cumulative spectrum of electrons, the electron ejection spectra from all the pulsars in the modelled globular cluster are summed up:

$$\Phi_{\text{el}} = \sum_{k=1}^{N_{\text{PSR}}} \Phi_{\text{el},k}(\gamma_{\text{el}}). \quad (12)$$

Examples of the cumulative electron spectra obtained for the population of millisecond pulsars residing in the synthetic globular cluster are presented in the *right* column of Fig. 3. The results for the cluster harbouring 20 synthetic millisecond pulsars is presented in the *top right* panel of Fig. 3. In the plot there are 25 different cumulative electron spectra Φ_{el} displayed. A common feature present in all of the spectra is a narrow peak positioned at high electron Lorentz factors. Its centre is around $\gamma_{\text{el}} \simeq 10^{6.5}$. A low energy tail is also characteristic of all the presented Φ_{el} spectra. It stretches down to electron Lorentz factors $\sim 10^4$. On average the particle flux level in the tail is two orders of magnitude lower than in the peak ($\Phi_{\text{el}} \sim 10^{25} \text{ s}^{-1} \text{ MeV}^{-1}$ in the tail versus $\Phi_{\text{el}} \sim 10^{27} \text{ s}^{-1} \text{ MeV}^{-1}$ in the peak). The shape of the tail is different between different globular cluster simulations. There are spectra where the tail is characterised by a type of plateau going from $\gamma_{\text{el}} \sim 10^5$ to 10^6 , which is followed by a sharp decline towards lower Lorentz factor values. There are also cases where the low energy tail declines steadily towards small γ_{el} values from the point it emerges from the high energy peak. The cumulative electron spectra Φ_{el} obtained for the synthetic globular cluster harbouring 100 millisecond pulsars are presented in the *bottom right* panel of Fig. 3. There are 10 different spectra Φ_{el} presented in the plot. Similarly as for the case of the cluster harbouring 20 pulsars, the narrow high energy peak is present in all of the simulated electron spectra Φ_{el} . It is centred at $\gamma_{\text{el}} \simeq 10^{6.5}$, and the maximum value of the particle flux is $\sim 10^{27.5} \text{ s}^{-1} \text{ MeV}^{-1}$. The average flux level in the low energy tail is by two orders of magnitude lower than in the peak. The shapes of the low energy tail are less diverse with respect to the case of the synthetic cluster with smaller pulsar population. In all simulated cases the tail declines steadily towards low γ_{el} values right from the point it emerges from the high energy peak. The particle flux level in the tail changes from $\sim 10^{26} \text{ s}^{-1} \text{ MeV}^{-1}$ at its high energy end ($\gamma_{\text{el}} \sim 10^{6.5}$) down to $\sim 10^{23} \text{ s}^{-1} \text{ MeV}^{-1}$ at its low energy end (γ_{el} between $\sim 10^4$ and $\sim 10^5$).

In order to simulate the inverse Compton scattering component to the γ -ray spectrum of the synthetic globular cluster, we are using a numerical model of the cluster developed by BS07. Because millisecond pulsars are concentrated in the cluster core, it is assumed in the model that the relativistic electrons (their distribution is given by Eq. 12) are injected in the centre of the globular cluster, and further they diffuse gradually towards outer parts of the cluster. The diffusion of particles is treated in the Bohm diffusion approximation. On their outward way, electrons interact with the cluster magnetic field, and also with ambient photon fields. BS07 (see fig. 1) showed that the radiation field within the GC and its nearby surrounding seems to be quite homogeneous. At the same time the electron diffusion distance mildly increases when moving towards the GC out-

skirts. Simple calculations show that the average diffusion distance for electrons injected in the cluster core and at its edge differ only by a factor of 2. Therefore the effect of distribution of pulsars within the core of globular cluster on the cluster's ICS emission is expected not to be very significant³ (taking into account the uncertainties of the discussed scenario).

Previously in their calculations, BS07 did not take into account synchrotron energy losses suffered by particles propagating through the cluster. In the presented calculations synchrotron losses are computed accordingly. However, the produced synchrotron radiation does not contribute to overall γ -ray emission of the cluster. The characteristic energies of the synchrotron photons produced by electrons escaping from the pulsar magnetospheres and propagating within the globular cluster are far below the γ -ray range. They can be estimated from $\varepsilon_{\text{char}} \approx m_{\text{el}} c^2 (B_{\text{GC}}/B_{\text{crit}}) \gamma_{\text{el}}^2$, where B_{crit} is the critical magnetic field (see e.g., Thompson & Duncan 1995). For the electrons with Lorentz factors of the order of 3×10^6 and the magnetic field strengths within GC of the order of $10 \mu\text{G}$, the synchrotron photons have characteristic energies in the optical range, i.e. they will be very difficult to observe due to the huge background from the GC stars.

In the calculations a following set of the globular cluster magnetic fields $B_{\text{GC}} = (0.3, 1.0, 3.0, 10, 30) \mu\text{G}$ is taken into account. A main source of photons permeating the cluster are stars residing in the cluster itself. The stellar photons can be up-scattered by the relativistic electrons (with energies up to $\sim 1 \text{ TeV}$) via inverse Compton scattering up to TeV energies. The density of the stellar radiation field is not constant throughout the cluster, but it should mimic the distribution of stars in the system. For this reason, the density of stars in the cluster is described in the framework of the Michie-King model (Michie 1963); this allows for determination of the energy density of stellar photons U_{stellar} as a function of the distance from the cluster centre. In order to determine the energy density of the stellar photons within the cluster information on the cluster visual luminosity L_{VIS} is necessary. Moreover, the core radius R_{c} , the half-mass radius R_{h} and the tidal radius R_{t} are also necessary for determining U_{stellar} in the cluster (see eqs. 4 and 5 of Bednarek & Sitarek 2007).

As shown by BS07, the energy density of the stellar radiation field ($U_{\text{stellar}} \approx 300 \text{ eV cm}^{-3}$ inside a cluster core for the case where core radius is 0.5 pc and cluster luminosity is at the level of $10^5 L_{\odot}$) dominates over the energy density of the cosmic microwave background (CMB; $U_{\text{CMB}} = 0.25 \text{ eV cm}^{-3}$). However, the latter photon field is important for estimating the ICS component (from tens MeV up to hundreds GeV) produced on the high energy electrons (energies above $\sim 1 \text{ TeV}$). The described processes are simulated using the Monte Carlo method, and lead to the production of the ICS

³ From the selected number of millisecond pulsars used to model synthetic γ -ray spectra of 47 Tuc and Ter 5 (see Sect. 5) only 5 out of 23 and 1 out of 31 (<http://www.naic.edu/~pfreire/GCpsr.html>), respectively, lie beyond the distance of $2 \times R_{\text{c}}$ but within the radius of $3 \times R_{\text{c}}$ (R_{c} is the cluster core radius). This is relatively small number. Thus, assuming that all MSPs are situated in the cluster core does not cause the ICS emission to be overestimated.

emission spectrum of the globular cluster. The details of the numerical code are presented in the work of BS07.

The results of the numerical simulations performed for two globular clusters: Terzan 5 and 47 Tucanae are presented in Sect. 5. The outcome of the simulations is the total γ -ray spectrum for each of the clusters. The spectrum consists of the magnetospheric and ICS component.

5 COMPARISON OF THE SIMULATIONS WITH THE OBSERVATIONS

Using the numerical procedure presented in Sect. 4, γ -ray spectra were computed for two selected globular clusters: Terzan 5 and 47 Tucanae. Where possible, the simulated spectra are compared with the publicly available observational data.

An important comment about the selection of pulsar periods for the population of MSPs residing in the clusters is necessary. Because for each of the selected clusters a number of millisecond pulsars was detected (see e.g., Ransom et al. 2005; Manchester et al. 1991; Camilo et al. 2000) and their spin periods were determined, a different approach to the problem of the spin period P selection than the one presented in Sect. 4 was used. From the list of the known MSPs in each cluster, pulsars with periods satisfying the criteria $P \lesssim 11$ ms were selected as the sole members of the population of the millisecond pulsars in the cluster. Knowing their spin periods and the density of the simulated grid in our database (Sect. 3.3), for each MSP the spin period value as close as possible to the true P value was assigned from the database. For each MSP the value of the magnetic field B_s and the inclination angle α was randomly selected from the discrete values simulated in our database (Sect. 3.3). From this point onwards, the procedure leading to the production of the cluster γ -ray spectrum matches the one presented in detail in Sect. 4.

5.1 The case of Terzan 5

Currently, Terzan 5 is the globular cluster with the largest number of the detected millisecond pulsars. There are 34 MSPs observed in the cluster (see the catalogue of P. C. Freire⁴). In addition, it is one of the first globular clusters detected in γ -rays by Fermi/LAT (Abdo et al. 2010; Kong et al. 2010). Its luminosity estimated in the energy range between 100 MeV up to around 20 GeV is $L_\gamma \simeq 2.6 \times 10^{35}$ erg s⁻¹ (Abdo et al. 2010) assuming the cluster is situated at a distance of $d \simeq 5.5$ kpc from the Sun. The observed γ -ray spectrum can be well fitted with a power law with an exponential cut-off $N(\mathcal{E}) \sim \mathcal{E}^{-\Gamma} e^{-\mathcal{E}/\mathcal{E}_c}$ ($N(\mathcal{E}) \equiv d\dot{N}_\gamma/d\mathcal{E}$ is a photon flux, Γ is a photon index, and \mathcal{E}_c is a cut-off energy). The spectral parameters estimated for Ter 5 are $\Gamma \simeq 1.4$ and $\mathcal{E}_c \simeq 2.6$ GeV (Abdo et al. 2010). Recently, the cluster has been detected by the H.E.S.S. telescope (Abramowski et al. 2011) in the TeV domain. The observed photon flux in the energy range above 0.4 TeV is $\simeq 1.2 \times 10^{-12}$ cm⁻² s⁻¹, while the photon index of the spectrum fitted with the power law $N(\mathcal{E}) \sim \mathcal{E}^{-\Gamma}$ is $\Gamma \simeq 2.5$. The

TeV emission detected from the direction of Ter 5 is slightly shifted with respect to the cluster core and it extends well beyond the cluster tidal radius. Abramowski et al. (2011) speculate that the observed TeV emission may be a source coincidence, e.g. with a PWN associated with a radio-quiet pulsar, or that the TeV γ -rays could have hadronic origin. If neither of these scenarios is true, then Ter 5 is the only globular cluster detected so far in the TeV domain with the Cherenkov telescopes.

Important parameters of Ter 5 cluster that are used in calculations of the ICS spectral component are the visual luminosity of the cluster $L_{\text{VIS}} \simeq 1.5 \times 10^5 L_\odot$ (Harris 1996). The core radius R_c , the half-mass radius R_h and the tidal radius R_t were taken from Harris (1996). The ambient photon fields up scattered via inverse Compton process are the cosmic microwave background ($U_{\text{CMB}} = 0.25$ eV cm⁻³) and the photons from the stellar population in the cluster (the energy density was estimated with eqs. 4 and 5 of BS07).

Out of 34 known MSPs in the cluster, 3 have spin periods larger than 11 ms. Thus, $N_{\text{PSR}} = 31$ were used to simulate γ -ray radiation from the cluster. The results are presented in Fig. 4. For one set of N_{PSR} with chosen (P, B_s, α) one cumulative spectrum of electrons (given by Eq. 12) is obtained. This spectrum is then injected into the cluster environment and it interacts with the ambient photon fields leading to the production of the ICS component of the γ -ray spectrum of the modelled globular cluster. Simultaneously, for one set of N_{PSR} many different cumulative magnetospheric spectra (given by Eq.10) are simulated. The cumulative magnetospheric spectrum is the component of the synthetic cluster γ -ray spectrum stretching from around MeV up to around few tens of GeV. The grey area in the *bottom* panel of Fig. 4 shows the region occupied by the group of different magnetospheric spectral components simulated for the cluster. It can be treated as the uncertainty of the GC emission spectrum in the MeV to GeV energy domain. In the *bottom* panel of Fig. 4 the simulated total γ -ray spectra for Ter 5 are presented with solid lines. To construct the total spectra, one magnetospheric component out of the simulated group was chosen. Five different ICS components were obtained for the cluster. They were simulated taking different values of the cluster magnetic field B_{GC} (see Sect. 4.3). For clarity, these ICS components are presented in the *top* panel of Fig. 4 separated from the chosen magnetospheric component.

The overall shape of the ICS spectral component (see the *top* panel of Fig. 4) can be described as having two peaks: the high energy peak (at photon energies above 1 TeV), and the low energy peak (at $\mathcal{E} \sim 10$ GeV). In the presented total GC spectra (the *bottom* panel of Fig. 4) only the high energy peak is visible, the low energy peak is dominated by the fading magnetospheric component of the cluster γ -ray emission. The ICS spectral component has slightly different shape and also different level depending on the cluster magnetic field values B_{GC} used in calculations (see Sect. 4.3). For low magnetic field strength in the cluster ($B_{\text{GC}} \lesssim 1 \mu\text{G}$) a clear dip between the high energy peak (resulting from IC scattering of the starlight photon field) and the low energy peak (resulting from IC scattering of the CMB) is visible. The dip gradually disappears when the magnetic field in the cluster increases ($B_{\text{GC}} > 1 \mu\text{G}$), leading to single peaked ICS spectrum for the case where $B_{\text{GC}} = 10$ and

⁴ <http://www.naic.edu/~pfreire/GCpsr.html>

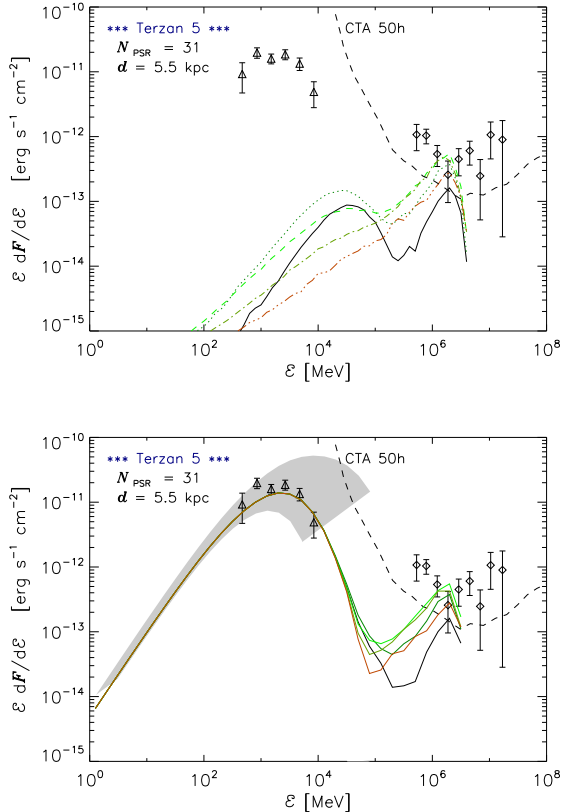


Figure 4. Synthetic spectra calculated for the globular cluster Terzan 5. The total number of millisecond pulsars in the cluster is $N_{\text{PSR}} = 31$. The distance to the cluster is assumed to be $d = 5.5$ kpc. *Top panel:* ICS spectra computed for different cluster magnetic field values B_{GC} . Solid black, green dotted, green dashed, green dot-dashed and brown dot-dot-dashed lines show models with B_{GC} of 0.3, 1.0, 3.0, 10, 30 μG , respectively. *Bottom panel:* Total γ -ray spectra (including magnetospheric and ICS component) are depicted with solid lines. Colours of the lines correspond to the value of the magnetic field in the globular cluster - from black, through shades of green to brown correspond to values of B_{GC} from 0.3 μG up to 30 μG . The colour-coding of the lines is the same as for the *top* panel. ICS spectra in the *bottom* panel were re-binned to match the resolution of the magnetospheric component spectra. Grey area shows the region occupied by the magnetospheric spectra of the cluster obtained for presented simulation runs (this can be treated as the uncertainty of the MeV to GeV emission spectrum of GC). Triangles show the γ -ray spectrum (with uncertainties) of Ter 5 as observed by the Fermi/LAT instrument (Abdo et al. 2010). Diamonds depict spectrum (and its errors) observed from the direction of the cluster by the H.E.S.S. telescope (Abramowski et al. 2011). Dashed line shows the CTA differential sensitivity curve with 50 h of integration (Actis et al. 2011).

30 μG . When we increase the B_{GC} value in the cluster, we see that the level of the ICS emission of the cluster increases. For the magnetic field values around 3 μG the emission reaches maximum. Further increase in B_{GC} results in the decrease of the emission level of the ICS component. This effect of the *increase-saturation-decrease* of the emission component resulting from the up-scattering of the stellar photon field and the CMB on the relativistic electrons diffusing

through the globular cluster environment can be explained by the synchrotron losses suffered by the electrons in the high magnetic fields. For low values of the magnetic field B_{GC} in the cluster, diffusion of electrons occurs rather fast ($t_{\text{diff}} \simeq 3 \times 10^{12}$ s for particles with energies $E_{\text{el}} = 0.1$ TeV, the cluster magnetic field $B_{\text{GC}} = 1$ μG and the cluster half mass radius $R_{\text{h}} = 1$ pc) and their IC cooling is less efficient. For strong magnetic fields particle diffusion is much slower ($t_{\text{diff}} \simeq 9 \times 10^{13}$ s for $B_{\text{GC}} = 30$ μG). However, as the B_{GC} increases, the synchrotron losses of the particles become larger leading to the saturation and decrease in production of the ICS photons.

In Fig. 4 the results of simulation for Ter 5 are also contrasted with the available observational data in the MeV to GeV (Fermi/LAT data; Abdo et al. 2010) and TeV (H.E.S.S. data; Abramowski et al. 2011) energy domain. With our simulations we obtain the magnetospheric γ -ray spectra that may reproduce or underestimate the cluster emission observed at energies below 10 GeV (see the results presented in the *bottom* panel of Fig. 4). However, we are unable to reproduce the exact spectral shape observed at TeV energies.

The γ -ray flux calculated in this paper should be considered as a guaranteed lower limit provided that the model for high energy processes occurring in the inner pulsar magnetosphere is correct. We conclude that TeV γ -ray observations of GCs can provide independent constraints on the pulsar models.

5.2 The case of 47 Tucanae

The 47 Tucanae globular cluster harbours 23 millisecond pulsars detected so far through radio searches (see e.g., Camilo & Rasio 2005; Manchester et al. 1991). Similarly to Ter 5, 47 Tuc has been detected in the MeV-GeV energy domain with the Fermi/LAT instrument (Abdo et al. 2010). Its γ -ray spectrum can be approximated with the exponentially cut-off power law with a spectral index $\Gamma \simeq 1.4$ and a cut-off energy $\mathcal{E}_c \simeq 2.2$ GeV. The cluster luminosity in this energy range is $L_{\gamma} \simeq 4.8 \times 10^{34}$ erg s^{-1} for the cluster distance d of 4.0 kpc. No TeV emission has been reported so far from 47 Tuc. However, the upper limit to the TeV emission of the cluster was estimated (Aharonian et al. 2009).

The 47 Tuc cluster visual luminosity is $L_{\text{VIS}} \simeq 7.5 \times 10^5 L_{\odot}$ (Harris 1996). The core radius R_c , the half-mass radius R_{h} and the tidal radius R_t were taken from Harris (1996). The ambient photon fields up scattered via inverse Compton process are the cosmic microwave background ($U_{\text{CMB}} = 0.25$ eV cm^{-3}) and the photons from the stellar population in the cluster (the energy density was estimated with eqs. 4 and 5 of BS07).

All of the detected 23 MSPs in 47 Tuc have spin periods smaller than 11 ms, so $N_{\text{PSR}} = 23$ in the simulations. The results are presented in Fig. 5. Similarly as for Ter 5, only high energy peak of the ICS component is visible in the cluster total spectrum (see the *bottom* panel of Fig. 5). The low energy peak, which is visible in the ICS spectra presented in the *top* panel of Fig. 5, is dominated by the magnetospheric component. The *increase-saturation-decrease* behaviour of the ICS emission component is visible, though the level difference between the ICS spectrum obtained for the lowest

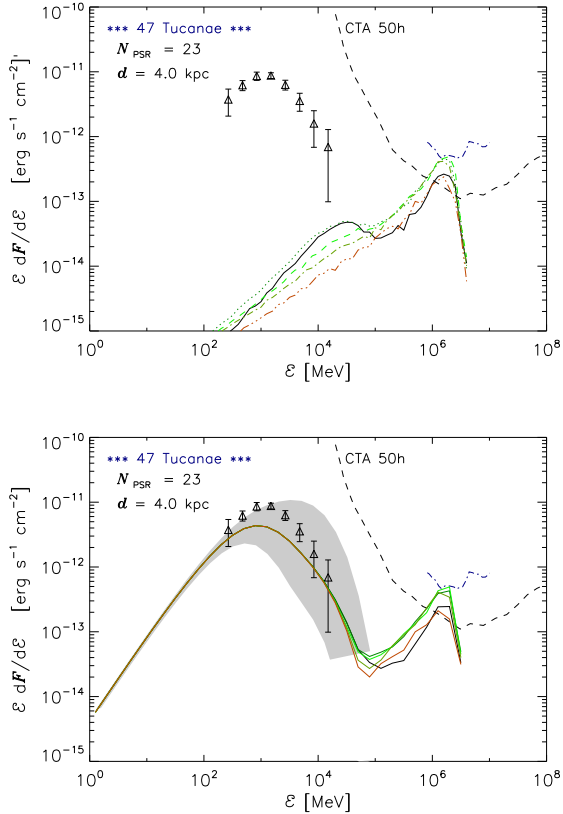


Figure 5. Same as Fig. 4 but for the globular cluster 47 Tucanae. Blue dot-dashed line represents the upper limit on TeV emission of 47 Tuc as obtained from H.E.S.S. telescope observations (Aharonian et al. 2009). Black dashed line shows the CTA differential sensitivity curve with 50 h of integration (Actis et al. 2011).

value of the magnetic field $B_{GC} = 0.3 \mu\text{G}$ and the spectra obtained for higher B_{GC} is smaller than in the case of Ter 5.

The simulated γ -ray spectra are compared with the available observational data from the Fermi/LAT instrument (Abdo et al. 2010). Our results rather nicely reproduce the cluster spectrum observed for energies $\lesssim 10$ GeV. As the cluster has not been detected in the TeV domain, we plot the H.E.S.S. upper limit (Aharonian et al. 2009). The modelled ICS spectral components do not violate the H.E.S.S. upper limit. The modelled TeV emission of 47 Tuc falls right below the presented upper limit. The differential sensitivity curve for the Cherenkov Telescope Array (CTA; Actis et al. 2011), the next generation system of Cherenkov telescopes, is also displayed in Fig. 5. The curve shows the CTA sensitivity obtained after 50 h of integration. Our simulations show that the cluster should be detectable with the CTA for all of the studied B_{GC} . However, the ICS emission is going to be more pronounced for the moderate values of the magnetic field within the cluster (B_{GC} between $1 \mu\text{G}$ and $10 \mu\text{G}$).

6 CONCLUSIONS

The γ -ray spectra (energies above ~ 100 MeV up to ~ 10 TeV) for synthetic globular clusters were calculated. The magnetospheric component (photon energies between ~ 100 MeV and ~ 30 GeV) of the cluster emission results from the cumulative γ -ray emission of millisecond pulsars residing within the cluster core. The ICS component (photon energies above ~ 30 GeV) is produced by the ambient photons (the stellar photon field originating from stars within the cluster, and the cosmic microwave background) up-scattered via inverse Compton process on relativistic electrons injected into the cluster environment from the synthetic MSP magnetospheres. The detailed simulations were performed for two globular clusters, Terzan 5 and 47 Tucanae, for which observational data are available in the energy range between MeV and TeV. Our calculations are able to reproduce, in both cases, the spectrum observed with the Fermi/LAT instrument for energies $\lesssim 10$ GeV (Abdo et al. 2009a, 2010). However, for Ter 5 where TeV observations are available, our simulations cannot account for the observed spectral shape in this energy domain.

On the other hand, it is possible that colliding pulsar winds, as proposed by BS07, can accelerate leptons to relativistic energies. Note that other compact objects within the GCs, such as rotating white dwarfs (Bednarek 2012) or accreting neutron stars, could be responsible for acceleration of electrons and their injection into the volume of GCs. The energy spectra of these shock-accelerated electrons are power-law in nature. Inclusion of this additional source of relativistic leptons - of different spectral character than the ones produced in MSP magnetospheres - into the calculations of ICS component could improve the match between the synthetic TeV spectrum calculated for Ter 5 and the H.E.S.S. observations (Abramowski et al. 2011). Thus, the calculated synthetic spectra of globular clusters at TeV energies should be treated as a lower limit to GCs emission in this energy range. This lower limit can be further tested by the future Cherenkov telescopes like CTA (Actis et al. 2011).

ACKNOWLEDGMENTS

This research was partially supported by NCN grants: 2011/01/N/ST9/00485, 2011/01/B/ST9/00411, and DEC-2011/02/A/ST9/00256.

REFERENCES

- Abdo A. A., Ackermann M., Ajello M., Fermi LAT Collaboration 2009a, *Science*, 325, 845
- Abdo A. A., Ackermann M., Ajello M., Fermi LAT Collaboration 2009b, *Science*, 325, 848
- Abdo A. A., Ackermann M., Ajello M., Fermi LAT Collaboration 2010, *A&A*, 524, A75
- Abramowski A., Acero F., Aharonian F., H.E.S.S. Collaboration 2011, *A&A*, 531, L18
- Actis M., Agnetta G., Aharonian F., CTA Consortium 2011, *Experimental Astronomy*, 32, 193
- Aharonian F., Akhperjanian A. G., Anton G., H.E.S.S. Collaboration 2009, *A&A*, 499, 273

- Anderhub H., Antonelli L. A., Antoranz P., MAGIC Collaboration 2009, *ApJ*, 702, 266
- Bednarek W., 2011, in Torres D. F., Rea N., eds, *High-Energy Emission from Pulsars and their Systems Gamma-rays from millisecond pulsars in Globular Clusters*. p. 185
- Bednarek W., 2012, *Journal of Physics G Nuclear Physics*, 39, 065001
- Bednarek W., Sitarek J., 2007, *MNRAS*, 377, 920
- Buesching I., Venter C., Kopp A., de Jager O. C., Clapson A. C., 2012, *ArXiv e-prints*
- Camilo F., Lorimer D. R., Freire P., Lyne A. G., Manchester R. N., 2000, *ApJ*, 535, 975
- Camilo F., Rasio F. A., 2005, in Rasio F. A., Stairs I. H., eds, *Binary Radio Pulsars Vol. 328 of Astronomical Society of the Pacific Conference Series, Pulsars in Globular Clusters*. p. 147
- Cheng K. S., Chernyshov D. O., Dogiel V. A., Hui C. Y., Kong A. K. H., 2010, *ApJ*, 723, 1219
- Cheng K. S., Ruderman M., Zhang L., 2000, *ApJ*, 537, 964
- Dyks J., 2002, PhD thesis, Centrum Astronomiczne im. M. Kopernika PAN
- Dyks J., Harding A. K., Rudak B., 2004, *ApJ*, 606, 1125
- Dyks J., Rudak B., 2002, *A&A*, 393, 511
- Eger P., Domainko W., Clapson A.-C., 2010, *A&A*, 513, A66
- Harding A. K., Muslimov A. G., 1998, *ApJ*, 508, 328
- Harding A. K., Usov V. V., Muslimov A. G., 2005, *ApJ*, 622, 531
- Harris W. E., 1996, *AJ*, 112, 1487
- Hui C. Y., Cheng K. S., Taam R. E., 2010, *ApJ*, 714, 1149
- Hui C. Y., Cheng K. S., Wang Y., Tam P. H. T., Kong A. K. H., Chernyshov D. O., Dogiel V. A., 2011, *ApJ*, 726, 100
- Ivanova N., 2006, *ApJ*, 636, 979
- Kong A. K. H., Hui C. Y., Cheng K. S., 2010, *ApJ*, 712, L36
- Manchester R. N., Lyne A. G., Robinson C., Bailes M., D'Amico N., 1991, *Nature*, 352, 219
- McCutcheon M., 2009, *ArXiv e-prints*
- Michie R. W., 1963, *MNRAS*, 125, 127
- Muslimov A., Harding A. K., 1997, *ApJ*, 485, 735
- Muslimov A. G., Harding A. K., 2004a, *ApJ*, 606, 1143
- Muslimov A. G., Harding A. K., 2004b, *ApJ*, 617, 471
- Muslimov A. G., Tsygan A. I., 1992, *MNRAS*, 255, 61
- Park S. K., Miller K. W., 1988, *Communications of the ACM*, 31, 1192
- Ransom S. M., Hessels J. W. T., Stairs I. H., Freire P. C. C., Camilo F., Kaspi V. M., Kaplan D. L., 2005, *Science*, 307, 892
- Rudak B., Dyks J., 1999, *MNRAS*, 303, 477
- Tam P. H. T., Kong A. K. H., Hui C. Y., Cheng K. S., Li C., Lu T.-N., 2011, *ApJ*, 729, 90
- Thompson C., Duncan R. C., 1995, *MNRAS*, 275, 255
- Venter C., De Jager O. C., 2005, *ApJ*, 619, L167
- Venter C., De Jager O. C., Clapson A.-C., 2009, *ApJ*, 696, L52
- Venter C., Johnson T. J., Harding A. K., 2012, *ApJ*, 744, 34
- Zajczyk A., 2008, *ArXiv e-prints*, 0805.2505
- Zajczyk A., 2012, PhD thesis, Centrum Astronomiczne im. M. Kopernika PAN and Université Montpellier 2